JOURNAL OF Materials CHEMISTRY

Synthesis and nonlinear optical properties of rod-like luminescent materials containing Schiff-base and naphthalimide units†

Yingchao Zhang,[a] Weihong Zhu,[a] Wenjun Wang,[b] He Tian,*[a] Jianhua Su[a] and Wencheng Wang[b]

[a]*Institute of Fine Chemicals, East China University of Science and Technology, Shanghai 200237, P. R. China. E-mail: tianhe@ecust.edu.cn; Fax: +86-21-64248311*
[b]*State Key Joint Lab for Materials Modification by Laser, Ion and Electron beams, Department of Physics, Fudan University, Shanghai 200433, P. R. China*

Received 15th October 2001, Accepted 27th February 2002
First published as an Advance Article on the web 26th March 2002

Two series of novel rod-like compounds containing Schiff-base and naphthalimide units were synthesized. The liquid crystalline and amorphous phases of these compounds have been studied by differential scanning calorimetry (DSC), polarizing microscopy and X-ray diffraction. It was found that compounds 1A, 2A and 3A with a bridge of benzene show an amorphous glassy state, whereas compounds 1B, 2B and 3B with 2,5-dioctyloxy-1,4-bis(phenylenevinylene)benzene as a bridge exhibit smectic F and nematic mesomorphic phases. These rod-like compounds emit yellow–green light with the photoluminescent peak at about 505 nm and have relatively high quantum yields. The nonlinear optical properties of the compounds have been investigated by using a second harmonic generation (SHG) technique on a Langmuir–Blodgett monolayer. Compound 3B exhibits SHG properties with a susceptibility $\chi^{(2)}$ of about 1.51×10^{-9} esu.

Introduction

Research into organic functional materials is an expanding area because of their interesting optical and electronic properties as well as their industrial applications in many fields including displays, electroluminescent (EL) devices, transistors, batteries, sensors and photoreceptors.[1–4] Materials possessing both self-organizing capability and fluidity properties can be used as active components in photorefractive materials,[5] liquid crystalline (LC) semiconductors,[6,7] and molecular wires and fibers.[8,9] Meanwhile, a great deal of light has been shed on amorphous materials due to their unique morphology.[10,11] The synthesis and application of novel materials which form stable amorphous glasses above room temperature have attracted considerable interest due to their excellent flexibility, transparency, non-existence of grain boundaries and isotropic properties.[12,13] Consequently, there is a strong interest in the application of organic light-emitting diodes (OLEDs) as light sources in the fast developing field of liquid crystal display (LCD) technologies. An approach to constructing OLEDs that emit linearly polarized light is the alignment of the emitting moieties in ultra-thin layers.[14] Alternatively, liquid crystalline fluorescent materials can be aligned on suitable alignment layers.[3]

The phenomenon of second-harmonic generation (SHG), whereby a material under illumination generates light at twice the incident frequency, is finding increasing use in the development of photonic devices.[15] Compared with traditional inorganic nonlinear optical materials, organic functional materials have several advantages, such as large birefringence and high dispersion of the refractive index.[16]The Langmuir–Blodgett (LB) technique is of interest because it permits control of the materials properties at the molecular level and it can make self-organized, non-centrosymmetric thin films , thus offering a way to create a non-centrosymmetric structure which is a prerequisite for SHG materials.[15,17] The LB-technique was first applied to the alignment of emission layers of conjugated light-emitting polymers by Neher and co-workers.[18]

Conventional Schiff-base compounds have limited use in many fields due to their low stability and poor solubility.[19] But Schiff-base compounds can offer compounds a highly polarisable π-electron conjugation system. It is known that crucial prerequisites for achieving large bulk second-order nonlinear optical (NLO) properties are that the individual constituents have large molecular NLO properties.[20] In addition, naphthalimide derivatives are well known to have a wide range of applications, such as, brilliant green–yellow dyes for synthetic polymer fibers,[21] supermolecular moieties for the study of photo-induced electron transfer,[22,23] and electroluminescent (EL) materials.[24–26] In this study, we incorporated a benzene-1,4-dicarboxaldehyde or a 2,5-dioctyloxy-1,4-bis(4-formylphenylenevinylene)benzene unit into a naphthalimide chromophore and synthesized six novel rod-like Schiff-base chromophores (shown in Scheme 1). In these compounds, Schiff-base units maintain liquid crystalline properties and potentially offer NLO properties, and the long terminal hydrocarbon chains improve the solubility and film-forming ability. With the alignment of these rod-like LCs the naphthalimide moiety could been utilized to orient fluorescent mesogens.

Results and discussion

1. Synthesis of rod-like Schiff-base molecules

The synthetic route to all these rod-like Schiff-base chromophores (shown in Scheme 1) is a modification of conventional preparation of Schiff-base compounds. According to the literature,[27,28] Schiff-base compounds can be prepared by condensing an amino group with an aldehyde group under reflux. The method we use here includes longer reaction times to allow the reaction to go further towards completion, using a catalyst and a stoichiometric excess of the amine moiety. In this way, after several recrystallizations from DMF we can obtain pure

†Electronic supplementary information (ESI) available: DSC of **2A** and **3B**, and a picture of the smectic F phase for **3B**. See http://www.rsc.org/suppdata/jm/b1/b109384n/

 DOI: 10.1039/b109384n

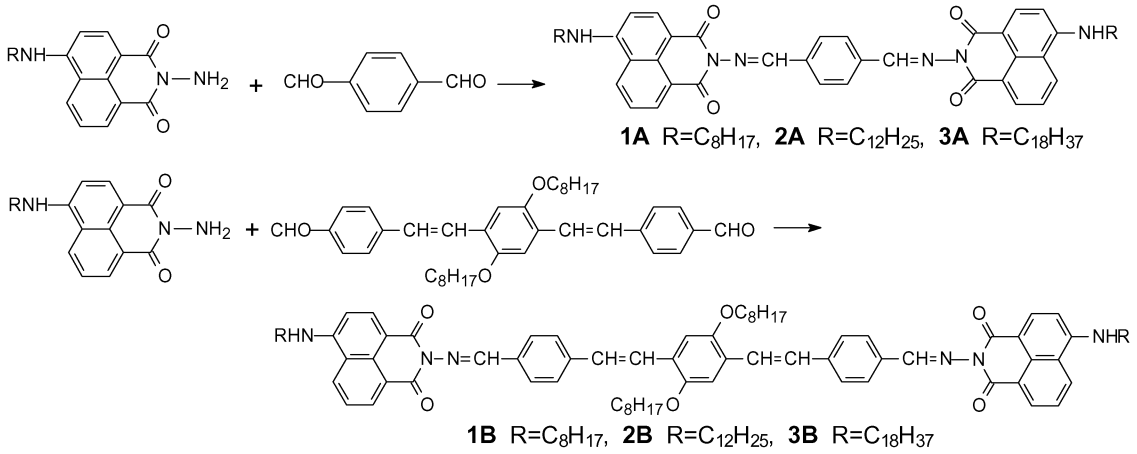

Scheme 1 Synthetic route of the target molecules.

(⩾99.5%) isolated target compounds with yields in the range of 72–88%.

The corresponding substituted naphthalimides were prepared *via* two steps from commercially available 4-bromo-1,8-naphthalic anhydride. Since 4-bromo-1,8-naphthalic anhydride has two reactive positions (the bromo and anhydride reactive centers), it has two possible reaction tendencies (either the bromo group is displaced or there is imidization) when it reacts with a primary amine. Fortunately, the reaction could be well controlled by choosing different solvents and reaction temperatures. According to the literature,[29,30] 4-bromo-1,8-naphthalic anhydride firstly reacts with hydrazine in a protic solvent (ethanol) at room temperature to give *N*-amino-4-bromo-1,8-naphthalimide with excellent yield, then *N*-amino-4-bromo-1,8-naphthalimide reacts with excess aliphatic amine in an aprotic solvent, *N*-methylpyrrolidin-2-one, at high temperature (110 °C) to give the desired products with a yield of 72–85%.

Based upon Wittig-type ethylenic group formation methodology, the intermediate 2,5-dioctyloxy-1,4-bis(4-formylphenylenevinylene)benzene could be prepared by the process depicted in Scheme 2. 1,4-Dioctyloxybenzene and 2,5-bis(bromomethyl)-1,4-dioctyloxybenzene could be similarly prepared according to the literature[31] with yields of 86% and 85%, respectively. As for the target intermediates, minor modifications[31] were made, such as using more lithium ethoxide solution and recrystallizing the desired compound from absolute ethanol instead of column chromatography. All of this simplified the procedure and resulted in good yields.

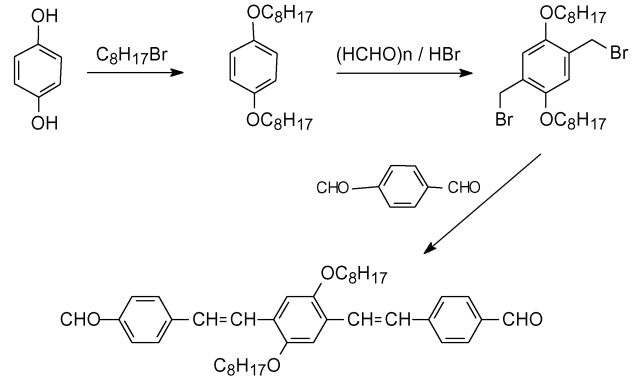

Scheme 2 Preparation of 2,5-dioctyloxy-1,4-bis(4-formylphenylenevinylene)benzene.

2. Spectral properties

As indicated in Table 1 and Fig. 1, the absorption peaks at about 435 nm correspond to the absorption of the naphthalimide moiety and the peaks of about 273 nm belong to the benzene moiety. It is evident that each of the compounds **1B**, **2B**, **3B** has an additional absorption peak of about 347 nm compared with compounds **1A**, **2A**, **3A**, which is attributed to the absorption of the conjugation system of phenylenevinylene. As found in Table 1, the fluorescent wavelength peaks of all these compounds show approximately the same value regardless of

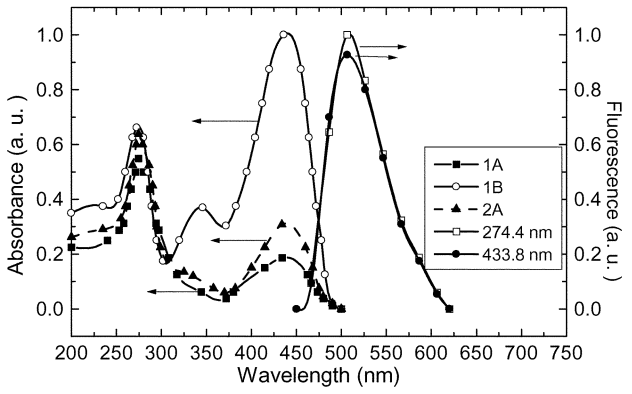

Fig. 1 Absorption spectra of compounds **1A**, **2A**, **1B** and the fluorescence spectra of compound **2A** (excited at 274 nm and 434 nm) in $CHCl_3$ (2.5×10^{-5} mol L^{-1}).

Table 1 The absorption and fluorescent spectral data of the compounds in $CHCl_3$ (2.5×10^{-5} mol L^{-1})

Compounds	1A	1B	2A	2B	3A	3B
λ_{max}^{ab}/nm (logε)	274 (4.72)	273 (4.81)	274 (4.79)	273 (4.80)	275 (4.86)	273 (4.78)
		346 (4.55)		348 (4.54)		348 (4.53)
	434 (4.27)	436 (4.98)	434 (4.47)	436 (4.97)	433 (4.56)	438 (4.97)
$\lambda^{em}{}_{max}$/nm (λ^{ex}/nm)	505.6 (274)	503.2 (346)	506.2 (274)	498.2 (347)	501.7 (275)	501.0 (347)
	507.5 (434)	499.8 (436)	506.7 (433)	497.3 (435)	501.1 (433)	502.3 (437)
Φ_{fl}*[a] (%)	77.9	76.4	94.6	70.7	68.8	78.3

[a]The relative fluorescence quantum yields (φ_{fl}) of these compounds were measured at room temperature by comparison with the standard of rhodamine 6G.

Table 2 Calorimetric data for compounds **1B**, **2B**, **3B**

Compounds	Phase	*T*/°C	Phase	*T*/°C	Phase	*T*/°C	Phase
1B	Cr	113	S	150	N	238	Is
2B	Cr	106	S	148	N	220	Is
3B	Cr	94	S	127	N	205	Is

the excited wavelength. A case in point is the spectrum of compound **2A** (shown in Fig. 1). All of these compounds emitted strong yellow–green fluorescence with high quantum yields. For example, compound **2A** has a high fluorescent quantum yield of 94.6% compared with a standard solution of rhodamine 6G. These materials are expected to find potential applications as functional materials, *e.g.* luminescent materials for photoreceptors and electroluminescent (EL) devices. The EL properties of these compounds are being investigated and the potential application of compounds **1B**, **2B** and **3B** in polarized electroluminescent devices will be studied in due course.

3. Mesomorphism and amorphous properties

Compounds **1B**, **2B** and **3B** exhibit liquid crystalline phases as evidenced by differential scanning calorimetry (DSC) and by the optical textures observed on a polarizing microscope equipped with a hot-stage apparatus. Table 2 depicts the calorimetric data for compounds **1B**, **2B** and **3B**. The symbols Cr, S, N and Is refer to the crystalline solid, smectic phase, nematic phase and isotropic liquid phase, respectively.

As seen in Table 2, compounds **1B**, **2B** and **3B** possess two kinds of mesophase, S and N phases. These mesogenics possess mesophases that exist over a large temperature range. For example, the nematic phase of compound **3B** was observed from 205 to 127 °C. This range is much larger than common Schiff-base LCs. This phenomenon is similar to the LC properties of some compounds containing a perylene core.[6,32] It is probably more accurate to say that, as the π-surface become larger, the enhanced stacking interactions increase stability, widening the temperature range. We have noticed that the transition temperature for these compounds is dependent on the chemical structure. The clearing temperature drops significantly as the number of carbons on the terminal group is increased. A case in point is that the clearing point of compound **3B** is 205 °C; 33 °C lower than that of compound **1B**. The phenomenon was also observed in other LC phase temperatures, such as the S phase temperature of compound **3B** which is 23 °C lower than that of compound **1B**. Within the temperature range of 127–94 °C for compound **3B**, a liquid crystal phase with high viscosity was observed by a polarizing microscope equipped with a hot-stage apparatus. Based on the knowledge concerning LC phases from the literature and our experience,[19] the observed phase should be referred to as a smectic F (S_f) phase, however, this conclusion can not yet be exactly confirmed in our lab by other measurements such as temperature-dependent wide- and small-angle X-ray patterns. Thermotropic behaviors were evaluated by means of DSC with at least two cycles (heating and then cooling refers to one cycle). Fig. 2 shows the DSC thermogram of compound **3B** on its second cooling and Fig. 4 is the thermogram of compound **2A** on its second heating.

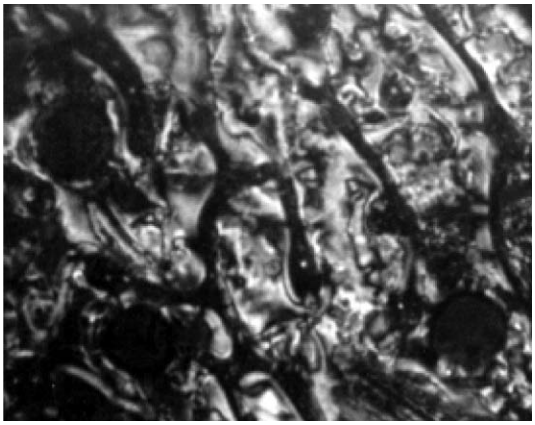

Fig. 3 Nematic phase texture of compound **3B**.

Representative DSC thermogram and nematic phase texture of compound **3B** are shown in Fig. 2 and 3, respectively. We observe three sharp exothermic peaks at 94 °C, 127 °C and 205 °C as shown in Fig. 2. It seems that the exothermic peaks at 94 °C and 127 °C refer to the LC phase transitions and another peak at 205 °C is due to the melting point (T_m). Referring to the Schlieren texture, the phases could be assigned to a nematic phase transition at 127 °C and a smectic phase transition at 94 °C. Compounds **1A**, **2A**, and **3A** have phase transitions evidenced by their TGA analysis and DSC thermograms. However, we can not observe their liquid crystalline phases under a polarizing microscope equipped with a hot-stage apparatus, but, when they were heated, melted, then cooled, they changed into the amorphous glassy state. Fig. 4 shows the DSC thermogram of **2A** on the second heating. The glass transition temperature (T_g) was observed at 32 °C, followed by an exothermic peak owing to crystallization at around 98 °C, then another crystallization occurred at 132 °C and the crystal melted at 295 °C. The formation of an amorphous glassy state is further evidenced by the X-ray diffraction pattern. As depicted in Fig. 5, compound **2A** showed no sharp signals but only broad halos at 20 °C, whereas several sharp signal peaks appeared at 120 °C which indicates that **2A** is in a crystalline state. Therefore compound **2A** has no liquid crystalline phase but an amorphous state.

From the molecular optimization structure calculated by

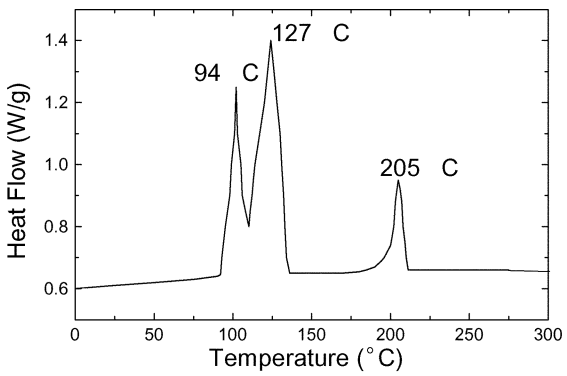

Fig. 2 Differential scanning calorimeter (DSC) traces of compound **3B** on the second cooling; the scan rate was 10 °C min^{-1}.

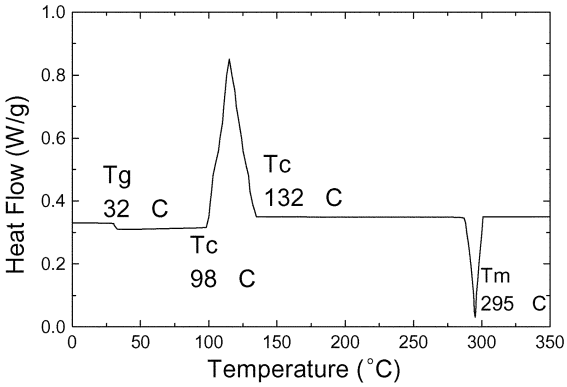

Fig. 4 Differential scanning calorimeter (DSC) traces of compound **2A** on the second heating. Scan rate was 10 °C min^{-1}.

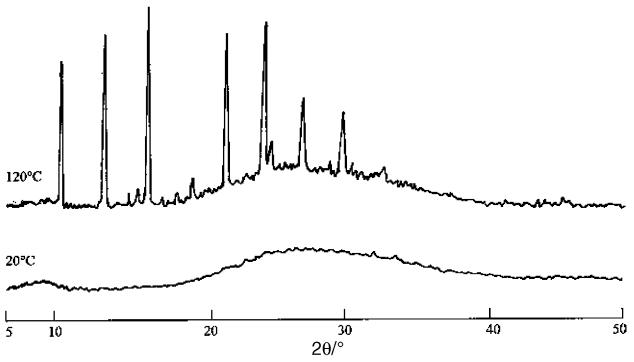

Fig. 5 X-Ray diffraction patterns of **2A** at 20 °C and 120 °C.

using a semiempirical molecular orbital package (MOPAC AM1 1997 release version) as shown in Fig. 6, it can be seen that these compounds are nonplanar. In this study we think that the nonplanar molecular conformation of **1A**, **2A**, and **3A**, together with the introduction of the long hydrocarbon chains at the 4-position of the naphthalimide prevent the easy spacial reorientation of the molecules, and consequently crystallization when cooled from the melting state. It thus favors the formation of a stable amorphous glassy state. For compounds **1B**, **2B** and **3B**, the increasing of the conjugation system and the introduction of long hydrocarbon chains to the 1,4-bis(4-formylphenylenevinylene)benzene moiety can decrease the strength of the steric hindrance, thus making such molecules more flexible. Hence they show liquid crystalline phases as conventional Schiff-base compounds.

4. Second-order nonlinear optical properties

Fig. 7 shows the surface pressure–area (π–A) isotherm of **3A** and **3B**. The steeply inclined part which corresponds to the formation of the solid monolayer, together with the high surface pressure of the collapse point of the monolayer indicate the good film-forming behavior of these compounds. From the surface π–A isotherm of **3B**, the monolayer collapse pressure is about 30 mN m^{-1} and the limiting area per molecule is estimated to be 180 $Å^2$. This indicates that the configuration of compound **3B** at the air–water interface is highly ordered. As for **3A**, the molecules at the air–water interface have a distinct

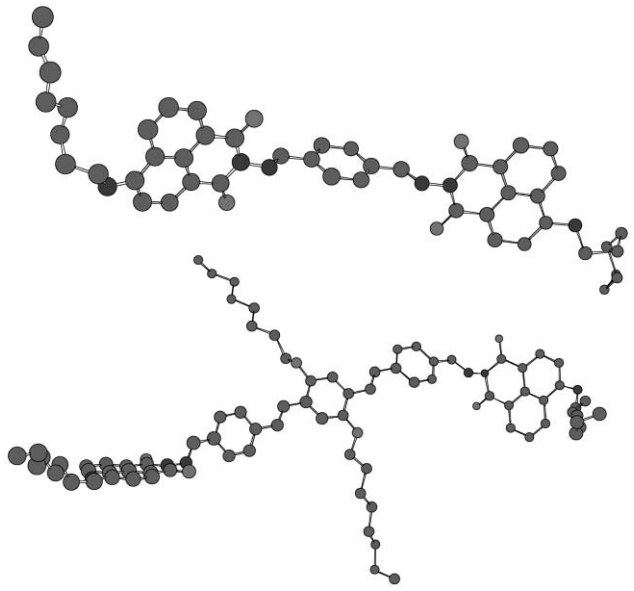

Fig. 6 Optimized molecular structure of compounds **3A** and **3B** calculated by using MOPAC AM1 methods.

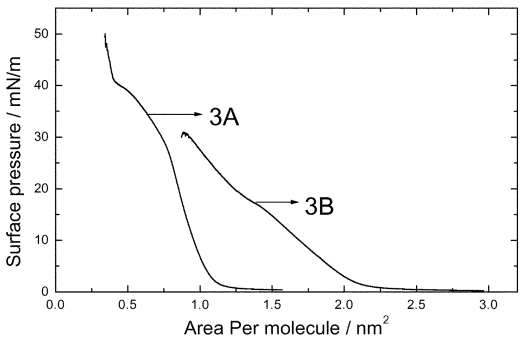

Fig. 7 π–A isotherm of compounds **3A** and **3B**.

solid phase part and the monolayer collapse pressure is over 40 mN m^{-1}. It was also assumed that the limiting area is larger for **3B** than for **3A**. Consequently, the molecules stand up on the surface as the surface pressure increases and the molecular area decreases, and the film eventually collapses.

In the SHG experiment, the macroscopic second-order susceptibility $\chi^{(2)}$ of the LB film of **3B** was determined by the method developed by Ashwell *et al.*[17]

$$I_{2\omega} = \frac{(\chi^{(2)} l I_\omega)^2}{n_\omega^2 n_{2\omega}} \quad (1)$$

Where l is the film thickness, I_ω is the incident beam intensity, and n_ω and $n_{2\omega}$ are the refractive indices at 1064 nm and 532 nm, respectively. The SHG signal from the **3B** monolayer was compared with the SHG signal from the reference quartz crystal for which $\chi^{(2)}$ is known (1.20×10^{-9} esu). The SHG measurements for **3B** and the reference were done under the same conditions for all controllable variables, taking $n_\omega = 1.51$ and $n_{2\omega} = 1.52$ for the reference quartz plate. The refractive indices for **3B** were taken to be $n_\omega = 1.57$ and $n_{2\omega} = 1.49$. Thus the second-order molecular hyperpolarizability (β) was then derived using the equation developed by Lupo *et al.*[33]

$$\beta = \frac{\chi^{(2)} l}{f^{2\omega}(f^\omega)^2 \sigma} \quad (2)$$

Here $f^{\omega,2\omega} = [(n^{\omega,2\omega})^2 + 2]/3$ is a local field factor, and σ is the surface density of the monolayer. Hence we can obtain $\chi^{(2)} = 1.51 \times 10^{-9}$ esu and $\beta = 2.3 \times 10^{-30}$ esu by comparison with the signal from the quartz reference and using the values above.

The measured *P*-in/*P*-out SHG intensity *vs.* incident angle is shown in Fig. 8(a) for the monolayers on both sides of the substrate. A maximum in intensity was obtained at an incident angle of 60°, which was close to results observed in previous work.[33,34] Notice that a clear fringe pattern was observed in Fig. 8(a). It is not a Maker-fringe because the sample thickness was much less than the SHG coherence length of the **3B** thin film. This pattern was caused by the interference between two internal SHG beams coming from the film on the front and back of the substrate. On the other hand, such a periodic fringe pattern disappears when a monolayer is on only one side as shown in Fig. 8(b). This phenomena gives the statement further evidence.

The SHG intensities of **3A** were also measured in the Langmuir–Blodgett films for pure **3A** Z-type 10 layers. But no SHG signal was observed. It is well known that an effective second-order NLO material needs to be noncentrosymmetric, which is a prerequisite for SHG materials. Comparing the optimization structural configuration between **3A** and **3B**, as shown in Fig. 6, we find that compound **3A** is almost centrosymmetric and **3B** is obviously noncentrosymmetric. We can assume that the origin of the SHG signals of **3B** is attributed to such noncentrosymmetry resulting from the incorporation of the 1,4-bisphenylenebenzene unit.

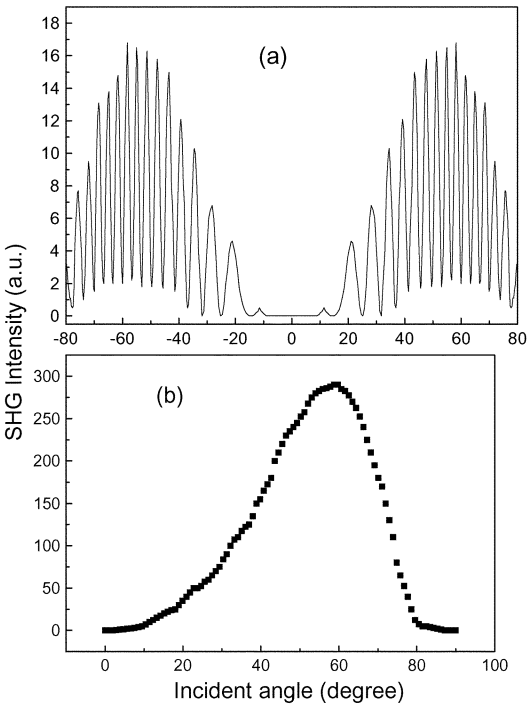

Fig. 8 SHG intensities as a function of incident angle for monolayers of compound **3B**: (a) monolayer on both sides of the substrate; (b) monolayer on one side of the substrate.

Experimental section

Infrared spectra were recorded on a Nicolet FTR-20sx, and ^{1}H-NMR spectra on a Brucker AM (500 MHz) NMR spectrometer using TMS as an internal standard. Absorption spectra were measured on a Shimadzu UV-260 spectrophotometer, and fluorescence spectra on a Hitachi-850 fluorescent spectrometer. Differential scanning calorimetry (DSC) was performed with a TA DSC 2910 instrument. Solvent toluene was dried over 4 Å molecular sieves for more than two days.

Synthesis of *N*-amino-4-octylamino-1,8-naphthalimide

N-Amino-4-bromo-1,8-naphthalimide can be readily prepared according to reference 24 with a yield of 92%, mp 218–220 °C (literature: 218–220 °C). A mixture of *N*-amino-4-bromo-1,8-naphthalimide (0.58 g, 2 mmol), 1-aminooctane (0.52 g, 4 mmol) and *N*-methylpyrrolidin-2-one (10 mL) was heated to 110 °C and stirred for 6 h under an argon atmosphere. After cooling, the mixture was poured into a mixture of ice and water, the solid was filtered and recrystallized from chlorobenzene, yielding bright yellow needles in 87% yield, mp 214–216 °C. ^{1}H-NMR (DMSO): δ(ppm) 0.88(t, 3H, C**H$_3$**-), 1.30(m, 12H,-(C**H$_2$**)$_6$-), 3.30(t, 2H, -NHC**H$_2$**-), 5.72(2H, N**H$_2$**), 6.80(d, J = 8.6 Hz, 1H), 7.70(d, J = 7.8 Hz, 1H), 8.32(d, J = 8.5 Hz, 1H), 8.46(d, J = 7.3 Hz, 1H), 8.72(d, J = 8.5 Hz, 1H).

Other *N*-amino-4-substituted 1,8-naphthalimide compounds were synthesized in a similar way. ***N*-Amino-4-dodecylamino-1,8-naphthalimide**: yield 92%. Mp 202–204°C. ^{1}H-NMR ($CDCl_3$): δ(ppm) 0.88(t, 3H, C**H$_3$**-), 1.18(m, 16H, -(C**H$_2$**)$_8$-), 1.56(m, 2H, -NHCH$_2$CH$_2$-C**H$_2$**-), 1.75(m, 2H, -NHCH$_2$-C**H$_2$**-), 3.45(t, 2H, -NH-C**H$_2$**-), 5.60(2H, N**H$_2$**), 6.80(d, J = 8.6 Hz, 1H), 7.68(d, J = 7.8 Hz, 1H), 8.20(d, J = 8.4 Hz, 1H), 8.45(d, J = 7.3 Hz, 1H), 8.70(d, J = 8.5 Hz, 1H). ***N*-Amino-4-octadecylamino-1,8-naphthalimide**: yield 95 %. Mp 194–196 °C. ^{1}H-NMR ($CDCl_3$): δ(ppm) 0.88(t, J = 6.9 Hz, 3H, C**H$_3$**-), 1.20(m, 28H, -(C**H$_2$**)$_{14}$-), 1.60(m, 2H, -NHCH$_2$CH$_2$-C**H$_2$**-), 1.70(m, 2H, -NHCH$_2$-C**H$_2$**-), 3.50(t, 2H, -NH-C**H$_2$**-), 5.65(2H, N**H$_2$**), 6.80(d, J = 8.6 Hz, 1H), 7.72(d, J = 7.8 Hz, 1H), 8.15(d, J = 8.3 Hz, 1H), 8.45(d, J = 7.3 Hz, 1H), 8.70(d, J = 8.5 Hz, 1H).

Synthesis of 1,4-dioctyloxybenzene

A suspension of 1,4-hydroquinone (2.75 g, 25 mmol), 1-bromooctane (14.48 g, 75 mmol), and K_2CO_3 (10.4 g, 75 mmol) in acetonitrile (50 mL) was heated at reflux for 2 days under an argon atmosphere before being poured into water (50 mL). The precipitates were firstly collected by suction and then dissolved in a minimum of hot hexane. Subsequently, the resulting hot solution was poured into methanol (50 mL) to give a white solid in 86% yield, mp 55–57 °C.

Synthesis of 2,5-bis(bromomethyl)-1,4-dioctyloxybenzene

To a suspension of 1,4-dioctyloxybenzene (0.7 g, 1.85 mmol) and paraformaldehyde (0.11 g, 3.80 mmol) in acetic acid (10 mL) was added hydrobromic acid (1.7 mL), then heated to 65 °C with stirring for 2 h. After cooling to room temperature, this suspension was poured into water (25 mL), the precipitate was filtered and dissolved in hot chloroform. Reprecipitation of the resulting solution in methanol then gave a white solid in 85% yield. Mp 74–76 °C. ^{1}H-NMR ($CDCl_3$): δ(ppm) 0.88(t, 6H, C**H$_3$**-), 1.28(m, 16H, -(C**H$_2$**)$_4$-), 1.48(m, 4H, -OCH$_2$C**H$_2$**-C**H$_2$**-), 1.81(m, 4H, -OCH$_2$-C**H$_2$**-), 3.98(t, 4H, -O-C**H$_2$**-), 4.52(s, 4H, C**H$_2$**Br), 6.85(s, 2H, aromatic ring).

Synthesis of 2,5-dioctyloxy-1,4-bis(4-formylphenylenevinylene)benzene

A suspension of 2,5-bis(bromomethyl)-1,4-dioctyloxybenzene (0.52 g, 1.0 mmol) and triphenylphosphine (0.55 g, 2.1 mmol) in toluene (30 mL) was heated at reflux for 3 h under an argon atmosphere. The solvent was then removed under reduced pressure. The resulting residue, along with benzene-1,4-dicarboxaldehyde (0.27 g, 2 mmol), was dissolved in methylene chloride (50 mL). To this solution was added lithium ethoxide solution (3 mL, 1.0 mol L^{-1} in ethanol) dropwise *via* a syringe at room temperature. The base should be introduced at such a rate that the transient red–purple color produced upon the addition of the base should not persist. The resulting solution was stirred for 20 min after the addition of the base and was then poured into a dilute aqueous hydrochloric acid. The organic layer was extracted, washed with water and dried over anhydrous sodium sulfate. The residue, after removal of solvent, was then crystallized from absolute ethanol to give a red, fluorescent solid in 81% yield. Mp 114–116 °C. ^{1}H-NMR ($CDCl_3$): δ(ppm) 0.89(t, 6H, C**H$_3$**-), 1.30(m, 16H, -(C**H$_2$**)$_4$), 1.55(m, 4H, -OCH$_2$C**H$_2$**- C**H$_2$**-), 1.86(m, 4H, -OCH$_2$-C**H$_2$**-), 4.05(t, 4H, -O-C**H$_2$**-), 7.15(s, 2H, central-phenyl-H), 7.42(d, J = 8.25 Hz, 2H, vinyl-H), 7.48(d, J = 8.28 Hz, 2H, vinyl-H), 7.75(m, 4H, phenyl-H), 7.85(m, 4H, phenyl-H), 10.10(s, 2H, C**H**=O).

General synthetic procedures of the target compounds. Into a 50 mL flask equipped with a Dean and Stark water distillation trap and a condenser were added the substituted naphthalimide (1 mmol), the dialdehyde (0.45 mmol), *p*-toluenesulfonic acid (0.05 mmol) and toluene (20 mL). The stirred reaction mixture was refluxed for 24 h and monitored by thin-layer chromatography (TLC). The yellow precipitate from the cooled reaction mixture was collected by suction, washed with toluene and dried, then crystallized from DMF to give bright yellow crystals.

Compound 1A. Mp >280 °C, yield 80%. IR (KBr): 3340, 2930, 2850, 1680, 1650, 1630, 1580, 1550, 1450, 1340, 1240, 820, 760, 720 cm^{-1}. ^{1}H-NMR ($CDCl_3$): δ(ppm) 0.88(t, 6H, C**H$_3$**-), 1.30(m, 20H, -(C**H$_2$**)$_5$), 1.65(m, 4H, -NHCH$_2$-C**H$_2$**-), 3. 45(t, 4H, -NH-C**H$_2$**-), 6.70(d, J = 8.7 Hz, 2H), 6.85(d, J = 8.6 Hz,

2H), 7.40(m, 4H, central-phenyl-H), 7.70(d, J = 8.4 Hz, 2H), 8.28(d, J = 7.3 Hz, 2H), 8.45(d, J = 7.3 Hz, 2H), 8.75(s, 2H, C**H**=N). MALDI-TOF-MS: [M^+] 775.49. Elemental analysis: Calc. for $C_{48}H_{52}N_6O_4$, C 74.22; H 6.70; N 10.82; Found: C 74.17; H 6.65; N 10.80%.

Compound 1B. Mp 238–240 °C, yield 76%. IR (KBr): 3350, 2930, 2850, 1680, 1650, 1630, 1570, 1540, 1450, 1340, 1240, 970, 910, 820, 760, 740, 720 cm^{-1}. ^{1}H-NMR ($CDCl_3$): δ(ppm) 0.88(m, 12H, C**H$_3$**-), 1.36(m, 40H, -(C**H$_2$**)$_5$), 1.75(m, 8H, -NHCH$_2$-C**H$_2$**- and -OCH$_2$-C**H$_2$**-), 3.40(t, 4H, -NH-C**H$_2$**-), 4.10(t, 4H, -O-C**H$_2$**-), 6.70(d, J = 8.5 Hz, 2H), 6.90(d, J = 8.4 Hz, 2H), 7.10(d, J = 8.2 Hz, 2H, vinyl-H), 7.15(d, J = 8.5 Hz, 2H, vinyl-H), 7.35(s, 2H, central-phenyl-H), 7.50(m, 4H, phenyl-H), 7.65(m, 4H, phenyl-H), 7.75(d, J = 8.3 Hz, 2H), 8.24(d, J = 7.9 Hz, 2H), 8.45(d, J = 8.2 Hz, 2H), 8.70(s, 2H C**H**=N). Elemental analysis: Calc. for $C_{80}H_{96}N_6O_6$, C 77.67; H 7.77; N 6.80; Found: C 77.57; H 7.75; N 6.83%.

Compound 2A. Mp >280 °C, yield 85%. IR (KBr): 3350, 2920, 2850, 1680, 1640, 1620, 1580, 1550, 1450, 1350, 1240, 820, 760, 720 cm^{-1}. ^{1}H-NMR ($CDCl_3$): δ(ppm) 0.88(t, 6H, C**H$_3$**-), 1.60(m, 36H,-(C**H$_2$**)$_9$), 2.62(m, 4H, -NHCH$_2$-C**H$_2$**-), 3.40(t, 4H, -NH-C**H$_2$**-), 6.70(d, J = 8.6 Hz, 2H), 7.20(d, J = 8.1 Hz, 2H), 7.45(m, 4H, central-phenyl-H), 7.60(d, J = 8.1 Hz, 2H), 8.25(d, J = 8.2 Hz, 2H), 8.50(d, J = 8.3 Hz, 2H), 8.72(s, 2H C**H**=N). MALDI-TOF-MS: [M^+] 888; [M^+ + 3], 891. Element analysis: Calc. for $C_{56}H_{68}N_6O_4$, C 75.68; H 7.66; N 9.46; Found: C 75.60; H 7.63; N 9.44%.

Compound 2B. Mp 220–222 °C, yield 74%. IR (KBr): 3350, 2920, 2850, 1680, 1650, 1620, 1570, 1540, 1460, 1340, 1240, 970, 910, 890, 820, 770, 740, 720 cm^{-1}. ^{1}H-NMR ($CDCl_3$): δ(ppm) 0.89(m, 12H, C**H$_3$**-), 1.40(m, 56H, -(C**H$_2$**)$_5$- and, -(C**H$_2$**)$_9$-), 1.80(m, 8H, -NHCH$_2$-C**H$_2$**- and -OCH$_2$-C**H$_2$**-), 3.35(t, 4H, -NH-C**H$_2$**-), 4.05(t, 4H, -O-C**H$_2$**-), 6.75(d, J = 8.5 Hz, 2H), 6.95(d, J = 8.4 Hz, 2H), 7.10(d, J = 8.2 Hz, 2H, vinyl-H), 7.15(d, J = 8.4 Hz, 2H, vinyl-H), 7.30(s, 2H, central-phenyl-H), 7.50(m, 4H, phenyl-H), 7.65(m, 4H, phenyl-H), 7.75(d, J = 8.2 Hz, 2H), 8.25(d, J = 7.8 Hz, 2H), 8.40(d, J = 8.2 Hz, 2H), 8.70(s, 2H C**H**=N). Elemental analysis: Calc. for $C_{88}H_{112}N_6O_6$, C 78.34; H 8.31; N 7.12; Found: C 78.27; H 8.35; N 7.10%.

Compound 3A. Mp 276–278 °C, yield 88%. IR (KBr): 3350, 2920, 2850, 1680, 1640, 1620, 1580, 1550, 1440, 1360, 1240, 830, 770, 720 cm^{-1}. ^{1}H-NMR ($CDCl_3$): δ(ppm) 0.88(t, 6H, C**H$_3$**-), 1.25(m, 56H, -(C**H$_2$**)$_{14}$), 1.70(m, 4H, -NHCH$_2$CH$_2$-C**H$_2$**-), 2.20(m, 4H, -NHCH$_2$-C**H$_2$**-), 3.40(t, 4H, -NH-C**H$_2$**-), 6.65(d, J = 8.7 Hz, 2H), 7.15(d, J = 8.1 Hz, 2H), 7.40(d, J = 8.1 Hz, 2H), 7.45(m, 4H, central-phenyl-H), 8.15(d, J = 8.2 Hz, 2H), 8.25(d, J = 8.2 Hz, 2H), 8.72(s, 2H, C**H**=N). Elemental analysis: Calc. for $C_{68}H_{92}N_6O_4$, C 77.27; H 8.71; N 7.95; Found: C 77.21; H 8.65; N 7.93%.

Compound 3B. Mp 205–208 °C, yield 72%. IR (KBr): 3360, 2930, 2850, 1680, 1650, 1630, 1570, 1540, 1460, 1340, 1240, 970, 910, 820, 760, 740, 720 cm^{-1}. ^{1}H-NMR ($CDCl_3$): δ(ppm) 0.88(m, 12H, C**H$_3$**-), 1.40(m, 80H, -(C**H$_2$**)$_5$- and -(C**H$_2$**)$_{15}$-), 1.80(m, 8H, -NHCH$_2$-C**H$_2$**- and -OCH$_2$-C**H$_2$**-), 2.80(t, 4H, -NH-C**H$_2$**-), 4.10(t, 4H, -O-C**H$_2$**-), 6.70(d, J = 8.5 Hz, 2H), 6.90(d, J = 8.4 Hz, 2H), 7.20(s, 2H, central-phenyl-H), 7.38(d, J = 8.3 Hz, 2H, vinyl-H), 7.45(d, J = 8.5 Hz, 2H, vinyl-H), 7.50(m, 4H, phenyl-H), 7.65(m, 4H, phenyl-H), 7.75(d, J = 8.2 Hz, 2H), 8.20(d, J = 7.9 Hz, 2H), 8.40(d, J = 8.2 Hz, 2H), 8.70(s, 2H, C**H**=N). Elemental analysis: Calc. for $C_{100}H_{136}N_6O_6$, C 79.68; H 8.97; N 5.54; Found: C 79.62; H 8.95; N 5.50%.

Determination of nonlinear optical properties

Surface pressure–molecular area (π–A) isotherm measurement and LB film deposition were all carried out on a KSV 5000 two-compartment Langmuir trough (made in Finland). Compounds **3A** and **3B** in different concentration toluene solutions were spread onto the aqueous subphase surface, then after waiting for 40–50 min for the solvent to evaporate, the floating film was compressed. The subphase was de-ionized with doubly distilled water at 20 °C. The surface pressure–area (π–A) isotherms were recorded at a barrier moving speed of 5 mm min^{-1}. Substrates (quartz) of size 30 mm × 18 mm × 2 mm were treated to obtain a hydrophilic surface. **3A** and **3B** were deposited during upstrokes at a dipping speed of 5 mm min^{-1}. Z-type multilayer films were deposited at a constant pressure of 15 mN m^{-1}. It took 5 minutes to dry the substrate after each deposition cycle. The transfer ratio could be displayed and automatically recorded by the computer during deposition.

The experimental setup used for SHG measurements has been described in reference 35. The incident fundamental beam of 35 ps pulse-width, 10 Hz repetition rate, 1.5 mJ $pulse^{-1}$ energy at a wavelength of 1.064 μm from a mode-locked Nd : YAG laser was directed onto the sample through a low filter which removed any second harmonic component in the incoming beam. The SHG signal at 532 nm was detected in transmission using a photomultiplier tube (PMT) and a boxcar averager, and recorded using a personal computer. The ratio of the SHG intensity from the samples to that from a z-cut quartz reference plate was taken to eliminate measurement errors caused by laser power fluctuations. The dependence of SHG intensity on the incident angle α was measured by rotating the samples in the incident plane.

Acknowledgement

This project was financially supported by NSFC/China (29836150) and Shanghai Education Committee. Authors thank Mr Min Zhao and Dr Dong Shen in ECUST for their help in making liquid crystal boxes.

References

1 G. P. Wiederrecht, B. A. Yoon and M. R. Wasielewski, *Science*, 1995, **270**, 1794.
2 C. W. Tang and S. A. VanSlyke, *Appl. Phys. Lett.*, 1987, **51**, 913.
3 M. Grell and D. D. C. Bradley, *Adv. Mater.*, 1999, **11**, 895.
4 H. Mochizuki, T. Hasui, M. Kawamoto, T. Shiono, T. Ikeda, C. Adachi, Y. Taniguchi and Y. J. Shirota, *J. Chem. Soc., Chem. Commun.*, 2000, 1293.
5 G. P. Wiederrecht, B. A. Yoon and M. R. Wasielewski, *Synth. Met.*, 1997, **84**, 901.
6 R. A. Cormier and B. A. Gregg, *Chem. Mater.*, 1998, **10**, 1309.
7 B. A. Gragg, M. A. Fox and A. J. Bard, *J. Am. Chem. Soc.*, 1989, **111**, 3024.
8 E. J. Osburn, A. Schmidt, L. K. Chau, S. Y. Chen, P. Smolenyak, N. R. Armstrong and D. F. O'Brien, *Adv. Mater.*, 1996, **8**, 926.
9 C. F. van Nostrum and R. J. M. Nolte, *J. Chem. Soc., Chem. Commun.*, 1996, 2385.
10 Y. Shirota, T. Kobata and N. Noma, *Chem. Lett.*, 1989, 1145.
11 W. Ishikawa, K. Noguchi, Y. Kuwabara and Y. Shirota, *Adv. Mater.*, 1993, **5**, 559.
12 H. Inada and Y. Shirota, *J. Mater. Chem.*, 1983, **3**, 319.
13 K. Katsuma and Y. Shirota, *Adv. Mater.*, 1998, **10**, 223.
14 D. Sainova, A. Zen, H. G. Nothofer, U. Asawapirom, U. Scherf, R. Hagen, T. Bieringer, S. Kostromine and D. Neher, *Adv. Functional Mater.*, 2002, **12**, 29.
15 G. J. Ashwell, R. C. Hargreaves, C. E. Baldwin, G. S. Bahra and C. R. Brown, *Nature*, 1992, **357**, 393.
16 H. Ai, Y. B. Fan, L. Tao, Y. Fang, F. G. Tao, G. M. Wang and W. C. Wang, *Thin Solid Films*, 1999, **350**, 219.
17 G. J. Ashwell, *J. Mater. Chem.*, 1999, **9**, 1991.
18 D. Neher, *Adv. Mater.*, 1995, **7**, 691.

19 *Topics in Physical Chemistry, Vol. 3 Liquid Crystals*, ed. H. Stegemeyer, Springer, New York, 1994.
20 M. Jalali-Heravi, A. Khandar and I. Sheikshoaie, *Spectrochim. Acta, Part A*, 1999, **55**, 2537.
21 A. T. Peters and M. J. Bide, *Dyes Pigm.*, 1985, **6**, 349.
22 A. P. de Silva, Q. N. Gunaratne, J. Habib-Jiwan, C. P. McCoy, T. E. Rice and J. P. Soumillion, *Angew. Chem., Int. Ed. Engl.*, 1995, **34**, 1738.
23 K. H. Hasharoni, S. R. Levanon, D. J. Greenfield, W. A. Svec Gostztola and M. R. Wasielewski, *J. Am. Chem. Soc.*, 1996, **118**(118), 10228.
24 K. Utsugi and S. T. Takano, *J. Electrochem. Soc.*, 1992, **139**, 3610.
25 Y. Chen, R. Wehrmann, A. Elschner and R. Dujardin, *DE 19,505,942* (1996).
26 W. H. Zhu, H. Tian and A. Elschner, *Chem. Lett.*, 1999, 501.
27 R. James and G. Jacques, *USP 4,057,569* (1977).
28 N. A. Vaz, S. L. Arora, J. W. Doane and A. D. Vries, *Mol. Cryst. Liq. Cryst.*, 1985, **128**, 23.
29 T. Xu, J. H. Su, K. C. Chen and H. Tian, *Heterocycl. Commun.*, 1999, **5**, 31.
30 T. Martynski, E. Mykowska, R. Stolarski and D. Bauman, *Dyes Pigm.*, 1994, **25**, 115.
31 B. Wang and M. R. Wasielewski, *J. Am. Chem. Soc.*, 1997, **119**, 12.
32 D. Pressner, C. Goeltner, H. W. Spiess and K. Müllen, *Ber. Bunsen-Ges. Phys. Chem.*, 1993, **97**, 1362.
33 D. Lupo, W. Prass and U. Scheunemann, *J. Opt. Soc. Am. B*, 1988, **5**, 300.
34 Y. Liu, Y. Xu, D. Zhu and T. Wada, *J. Phys. Chem.*, 1995, **99**, 6957.
35 W. J. Wang, J. H. Xu, Y. Q. Jiang and X. Z. Lu, *Thin Solid Films*, 2000, **365**, 116.